Ecological Informatics 98 (2026) 103973

Contents lists available at ScienceDirect

Ecological Informatics

journal homepage: www.elsevier.com/locate/ecolinf

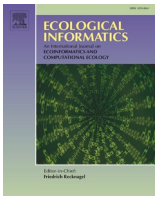

Leveraging foundation models and time-lapse photography for semi-automated tracking of tree apical growth

Lynsay Spafford [a,*], Louis Duchesne [b], Vivien Sainte Fare Garnot [c], Jacob Ravn [a], Loïc D'Orangeville [a,d]

[a] Faculty of Forestry and Environmental Management, University of New Brunswick, 28 Dineen Dr, Fredericton, NB E3B 5A3, Canada
[b] Direction de la recherche forestière, Ministère des Ressources naturelles et des Forêts du Québec, 2700 Einstein St, Québec, QC G1P 3W8, Canada
[c] Department of Mathematical Modeling and Machine Learning (DM3L), University of Zurich, 190, Winterthurerstrasse, 8057 Zürich, Switzerland
[d] Département des sciences du bois et de la forêt, Laval University, 2405 De la Terrasse St, Québec City, QC G1V 0A6, Canada

ARTICLE INFO

Keywords:
Segment Anything Model Version 2 (SAM2)
Primary growth
Time-lapse photography
Intra-seasonal growth
Image segmentation
Forest productivity

ABSTRACT

Primary growth is a key determinant of tree seedling survival, competition, forest composition, and productivity. Despite its importance, no established in-situ techniques currently exist for efficiently tracking fine-scale height growth. To address this, we developed a semi-automatic approach using time-lapse images and the Segment Anything Model v2 (SAM2; Meta AI Research) to quantify conifer apical growth. We obtained image time series of 105 apical balsam fir leaders from two sites in Québec, Canada, collected over 13 growing seasons, using two different camera types, with background varying from other trees to the sky. We used SAM2 with manual prompts to segment leaders within image time series. We measured the length of each segmentation and applied a post-processing step to address potential erroneous segmentations. Leader lengths derived from SAM2 concurred with independent manual reference measurements ($R^2 = 0.984$, 8309 images) which took 20 times longer to acquire (one hour) versus the SAM2 approach (three minutes one second) on average per series. Agreement between SAM2 and manual growth series for the timing of 75% growth amplitude was moderate ($R^2 = 0.57$) and could be augmented with mask revisions. This cost-effective fine-scale monitoring framework could be applied to track seedling, sapling, and stand-level growth. It also could augment evergreen primary growth tracking in phenocam networks and provide reference measurements for large-scale remote sensing programs. By enabling the development of intra-seasonal height growth profiles, this approach could support the identification of climate-resilient species and provenances.

1. Introduction

As cells divide in the apical meristem of terminal buds, tree stems elongate, resulting in primary growth. The primary growth of terminal leaders of trees plays a critical role for seedlings and saplings, determining light access, competition, and survival (Claveau et al., 2002; Kattenborn et al., 2017; Kneeshaw et al., 2006; Niinemets and Valladares, 2006; Thomas et al., 2024). At larger scales, differences in height growth rates during stand initiation and stem exclusion can shape the future composition of stands and are a key determinant of forest productivity. In mature stands, height growth continues to play an important role in influencing canopy structure and competition, with growth rates differing among species and responding to gap formation events more than 20 m away in boreal forests (Vepakomma et al., 2011).

Studies of high-frequency radial growth records from electronic dendrometers have revealed that radial growth rates can vary dynamically throughout a growing season or even over diurnal periods due to fluctuations in air temperature, moisture availability and vapour pressure deficit (Duchesne et al., 2012; Etzold et al., 2022; Oogathoo et al., 2024; Thivierge-Lampron et al., 2025; Zweifel et al., 2016; Zweifel et al., 2021a, 2021b). Studies based on both high-frequency and low-frequency tree radii records have revealed distinct phenologies between species with important implications for forest productivity and climate resilience (Aldea et al., 2018; Aldea et al., 2021; D'Orangeville et al., 2022; Pappas et al., 2020; van der Maaten et al., 2018). In contrast, there are no widely used techniques for high-frequency in-situ

* Corresponding author.
E-mail addresses: lynsay.spafford@unb.ca (L. Spafford), louis.duchesne@mrnf.gouv.qc.ca (L. Duchesne), vsaint@ics.uzh.ch (V.S.F. Garnot), jravn@unb.ca (J. Ravn), Loic.Dorangeville@sbf.ulaval.ca (L. D'Orangeville).

https://doi.org/10.1016/j.ecoinf.2026.103973
Received 9 March 2026; Received in revised form 3 August 2026; Accepted 4 August 2026
Available online 5 August 2026

tracking of height growth, and height growth tracking of seedlings and saplings typically necessitates time-consuming manual field measurements with rulers. As a result, tree height growth phenology is underexplored relative to radial growth phenology. Given the importance of height growth in affecting tree survival, future stand compositions, and forest productivity, novel measuring techniques are needed to facilitate height growth data acquisition. This would allow for the establishment of species-specific height growth phenology profiles and quantification of height growth responses to environmental drivers throughout life stages.

Obtaining high-quality measurements of seedling, sapling, and tree height growth over time poses several challenges, as fine-scale changes on the order of centimetres require sensitive and precise measurement methods. Additionally, as these changes occur over successive days within a growing season, frequent monitoring at the daily scale is necessary to capture the timing and magnitude of ongoing changes. Such monitoring frequency and precision are impractical for manual height tracking approaches using rulers for seedlings and saplings, and clinometers for mature trees. Remote sensing methods, including medium-range terrestrial laser scanning and satellite-based LiDAR, likewise face limitations in tracking fine-scale daily height growth methods (Kershaw et al., 2016; Yrttimaa et al., 2022).

The widespread availability and affordability of consumer-grade time-lapse cameras offer new potential for near-continuous monitoring networks. Coupled with recent advances in deep learning foundation models, such as the Segment Anything Model v2 (SAM2) developed by Meta AI, this provides increasing opportunities for precise and semi-automated height growth monitoring by tracking the spatial extent of young trees and branches in image time series. The open-source SAM2 is a transformer-based foundation model trained on an extensive and diverse dataset of 11 million images with 1.1 billion masks (Hu et al., 2023; Olsson, 2024; Ravi et al., 2024). It includes a Vision Transformer (ViT), a type of deep learning architecture that uses self-attention mechanisms to detect relationships among pixel elements. This enables the encoding of image pixels into meaningful visual features, and the capture of global relationships within images, such as between parts of a seedling. Due to the vast number of segmentation masks it has been trained on, SAM2 can produce accurate segmentation masks on unseen images. Furthermore, these segmentations can be guided by additional prompts to improve accuracy. Unlike its predecessor, SAM1 (version 1), which was designed solely for static image segmentation, SAM2 incorporates a dynamic memory mechanism that retains features and prompts from earlier frames in a video or time-lapse sequence to improve object segmentation in subsequent frames. Previously, SAM1 has been applied to a variety of forestry-related applications, including building segmentations from orthophotos (Hattula et al., 2025), forest structure and tree crown segmentation (Que et al., 2026; Wołk et al., 2025), and forest disturbance detection (Tian et al., 2025). In video or time-series applications, SAM2 has typically been used for objects that remain constant in size and shape, and its effectiveness for tracking dynamic objects, such as emerging tree leaders, remains unknown. In addition, SAM2 has been found to confuse similar-looking objects, and its capacity to distinguish one leader from other nearly identical leaders within the same frame is also unknown. Further, Rana et al. (2026a, 2026b) demonstrated that reliable deployment of computer vision systems in field environments requires evaluation of robustness to occlusion, lighting heterogeneity, image quality, as well as error-oriented reliability metrics such as bias and per-series error metrics. These considerations are especially relevant to forestry applications in visually complex environments which vary over daily and seasonal time scales.

In this study we aimed to develop a semi-automated pipeline using time-lapse photography and SAM2 to monitor fine-scale primary growth in balsam fir (*Abies balsamea* (L.) Mill.). We selected balsam fir for these tests due to its strong apical dominance, which results in a single, clearly visible terminal leader, and due to the availability of a sub-daily high-resolution image (12 MP) archive spanning 13 growing seasons. The monitored trees varied in terms of social positions and background compositions. Backgrounds ranged from predominantly other balsam fir trees, making leader distinction challenging, to a combination of other balsam fir trees and skyline, and to pure sky, simulating the diverse conditions typical of young forest stands. Our goal was to accurately and reliably track fine-scale apical growth in balsam fir, regardless of tree social position or background complexity, providing measurements comparable to those obtained through manual observations. Consistent with recommendations from Rana et al. (2026a, 2026b) we selected optimal configurations and evaluated performance using error-oriented and per-series reliability metrics capturing robustness under varying lighting, occlusion, and background conditions.

2. Materials and methods

2.1. Study site location

The apical growth of young natural balsam fir trees was monitored using time-lapse photography over a 13-year period at two sites with open lighting conditions (LLEC: 47.324° N, 71.126° W; LLFM: 47.313° N, 71.128° W, 1.2 km apart) near the Lake Laflamme study watershed, within Montmorency Forest, 70 km north of Québec City (Quebec, Canada). The mean annual temperature in the area is 0 °C, and the mean annual precipitation is 143 cm for the 1991–2020 period.

2.2. Camera configuration

At the LLEC site, trees were monitored from 2012 to 2020 with an 8-megapixel camera (Stealth Cam, model WF097C, GSM Outdoors, Irving, Texas, USA; image size 3264 × 2448 pixels). Additionally, another Stealth Cam camera (model G42NGNC; image size 4000 × 3000 pixels) was used in 2017 and 2018, positioned near the 8-megapixel camera to capture trees outside the primary camera's frame. At the LLFM site, trees were monitored from 2018 to 2024 with a 12-megapixel camera. A Stealth Cam camera (model G42NGNC) was used from 2018 to 2023, and a Spypoint camera (model SOLAR, GG Telecom, Victoriaville, Québec, Canada; image size 4000 × 3000 pixels) was used in 2024.

Each spring, cameras were mounted on a metal tripod tower at approximately the same height as the apical buds of the monitored trees. These cameras were positioned at a distance that allowed the apical growth of at least ten trees to be captured in the field of view. Example fields of view for cameras at each site are shown in Fig. 1. Images were taken every hour from early morning to early evening (05:00–06:00 to 19:00–20:00, depending on the year), from mid-May (15–25 May) until at least the end of August (15–31 August). At the LLFM site, cameras were installed later in the season in 2019 and 2020 (on June 4 and 15, respectively). In 2023, a power supply failure caused image capture to stop on August 7, although a photo taken on October 16 allowed the annual apical growth of the monitored trees to be measured. One clear image per day was selected, with image times ranging from 05:00 to 19:00. If no clear images were available for a given day, that day was skipped. Early morning or late-day images were preferred because apical leaders tend to be more erect at these times compared to midday when they often bend, particularly on hot, sunny days. Occasional gaps occurred due to camera malfunction. A total of 1669 daily images were amassed over the 13-year period.

At the LLEC site, 12 to 16 trees were selected each year from 2012 to 2017. After observing a high degree of synchronicity in the seasonal growth patterns of individual trees, only five to seven trees were selected each year from 2018 to 2020. At the LLFM site, five trees were monitored annually. Across both sites we amassed a total of 137 annual tree series over the 13-year monitoring period. Of these, we selected 105 series for analysis with SAM2. We excluded series in which the bud or leader was blocked by other trees or was difficult to distinguish from background elements making SAM2 guidance prompt delineations less well defined. Our selected leaders spanned a range of social positions

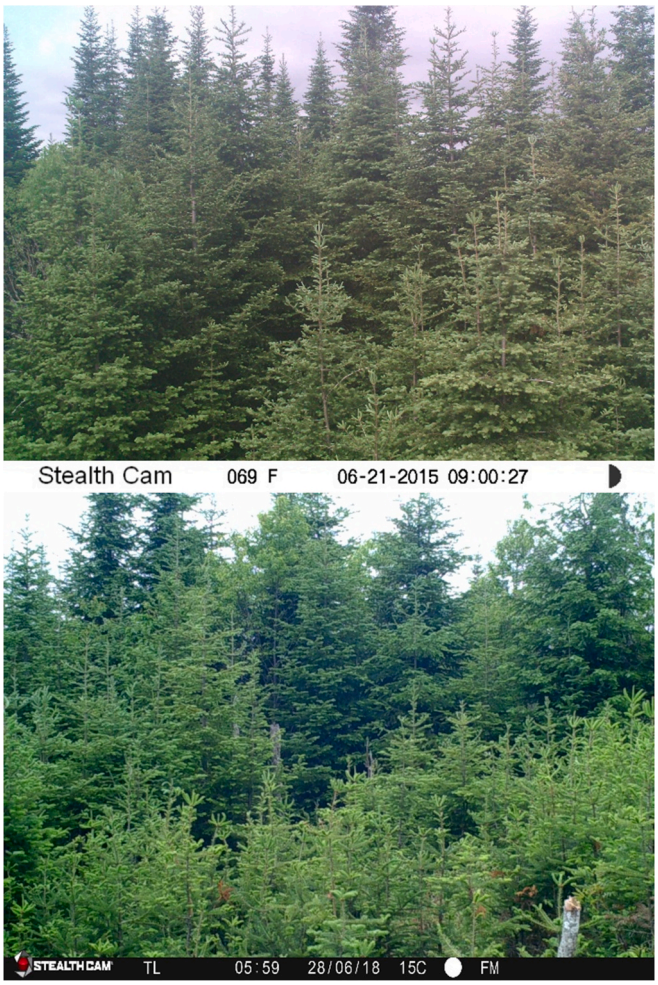

Fig. 1. Example field of view from the Stealth Cam model at the LLEC site (top) and the LLFM site (bottom).

within the monitoring plots, with some belonging to relatively young and short trees in the foreground, and others to dominant older trees along the skyline. Background for leaders varied from dense balsam fir branches, which made distinguishing the target leader more challenging, to just pure sky, which made distinction of the target leader easier. This combination of varying contexts in terms of size, proximity to the camera, and background, provided a broad range of conditions for evaluating our SAM2 growth monitoring approach.

2.3. Image processing & SAM2-based segmentation

2.3.1. Overall pipeline

To obtain length estimates of leaders over time, we used SAM2 (Segment Anything Model 2; Meta AI Research, available at https://github.com/facebookresearch/sam2; Ravi et al., 2024) to segment each target leader throughout an image time series. We then extracted the length of the segmented leader in each image in units of pixels. We conducted a sensitivity ablation analysis to optimize the steps of our pipeline, as described below and in Table 1. To evaluate the length estimates, we compared them with measurements derived manually from image time series using either the Adobe Illustrator or Image J software. An overview of the complete pipeline for obtaining leader length estimates from image time series with SAM2 is presented in Fig. 2. Prior to adopting SAM2, we conducted preliminary tests using SAM version 1 with image-by-image click prompting. This approach required substantial user interaction and produced less consistent segmentations over image series. This motivated our use of SAM2 and the subsequent development of the workflow evaluated in this study.

Table 1
Parameter ranges and optimal values resulting from our sensitivity ablation analysis.

Parameter	Configurations Tested	Optimal Configuration
Box prompt frequency	5, 10, 20	5
Number of Negative Point Prompts	0, 1, 2	2
Relative Outlier Threshold	None, 0.2, 0.4, 0.6, 0.8, 1.0, 1.2, 1.4, 1.6, 1.8, 2.0, 2.2, 2.4, 2.6, 2.8, 3.0 times maximum length	1.8
Phase splitting	Yes or No	Yes
Merging mask fragments	Yes or No	Yes
Smoothing method	None; spline smoothing with *p* parameter 1, 2, 5, or 20; median rolling-window over 3, 5, 7, 10, or 14 days; Gompertz with B growth rate parameter 3, 5, or 7; Weibull with C shape parameter 1.5, 2.0, or 3.0	Weibull with C parameter 3.0

2.3.2. Sensitivity ablation analysis

To optimize the parameter values for our SAM2 processing pipeline, we conducted a combined sensitivity ablation analysis on six processing steps. Table 1 indicates the processing step configurations we tested and the resulting optimal values. We tested a total of 9,792 unique prompting and processing configurations for all leader series, totalling 1,028,160 leader runs. Optimal values were selected using bootstrapping with 105 leader series sampled with replacement 1,000 times. For each iteration, configurations were ranked separately for each leader series based on absolute error in the prediction of the timing of 50% of maximum length attained. When there was a tie between configurations, the root mean squared error (RMSE) between SAM2 and manual reference lengths for each image in units of pixels was used as a secondary criterion for ranking. The configuration with the lowest mean rank across leader series was then used to determine the optimal configuration. This approach helped to ensure that the selected optimal configuration was robust to leader series sampling bias. Further, following the recommendations of Rana et al. (2026a), we adopted this per-series optimization approach to capture robustness under different scenes and background conditions. To determine how our selected optimal configuration generalized to unseen years and sites within our dataset, we conducted leave-one-year-out and leave-one-site-out validations. For both validations we quantified configuration rankings for training and testing groups and the agreement between group rankings was determined using Spearman's rank correlation. Our hold out validations indicated that configuration rankings were moderately to well preserved between training and hold out sites and years (Spearman's $\rho = 0.45$–0.84 for years, 0.79 for sites). The complete performance and time results for all configurations are included in the accompanying data repository.

2.3.3. Reference prompts and propagation

To initialize SAM2-based segmentation, we cropped a time series of images for each leader of interest, so that the leader and the preceding dormant bud were clearly visible throughout. This cropping substantially reduces processing time in applying SAM2, though does not eliminate the potential for other non-target leaders to be present in cropped image frames, see for example Fig. 4. To load the SAM2 video predictor we used the Hiera-Large hierarchical Vision Transformer backbone (sam2.1_hiera_large) from the official pretrained checkpoint and configuration files (https://github.com/facebookresearch/sam2). We added guiding prompts to the SAM2 video predictor to track each leader or bud on a sequence of images every five days. Each guiding

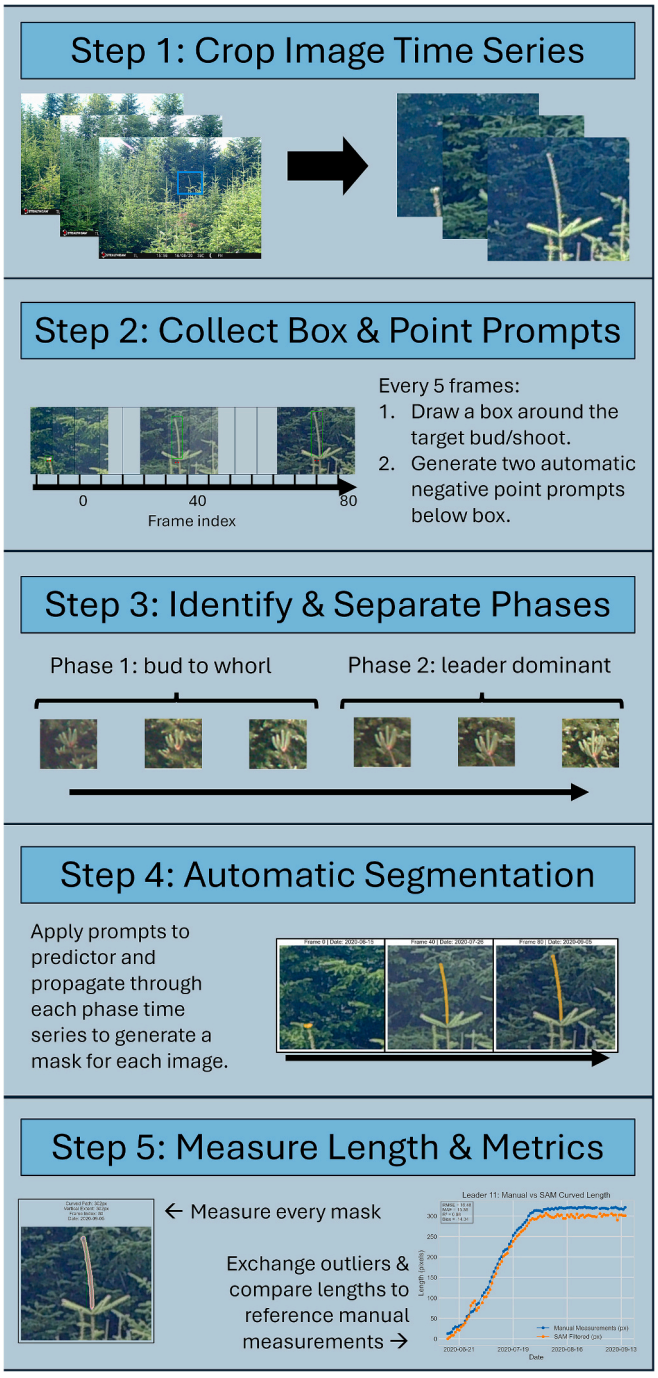

Fig. 2. Pipeline for obtaining leader length estimates with SAM2 from image time series.

prompt consisted of a box prompt drawn over the extent of the leader or bud and two negative point prompts. These point prompts were positioned 10% of the box height below the box and evenly spaced across its lateral extent, as illustrated in Fig. 3. We included these negative point prompts to suppress the inclusion of parts of the tree stem from a previous year's growth in the segmentations for a given growing season. The optimal frequency of guiding prompts and the optimal number of negative point prompts were determined through a sensitivity analysis, summarized in Table 1.

We then split our prompts into two phases: an early phase (phase one) and a late phase (phase two) because the shape and appearance of the target changed substantially between phases (Fig. 4). In phase one, dormant buds swell and shoots emerge, with the target leader being as

Fig. 3. Example box prompt and semi-automatic negative point prompts to guide SAM2 segmentation of the leader of interest from a cropped image.

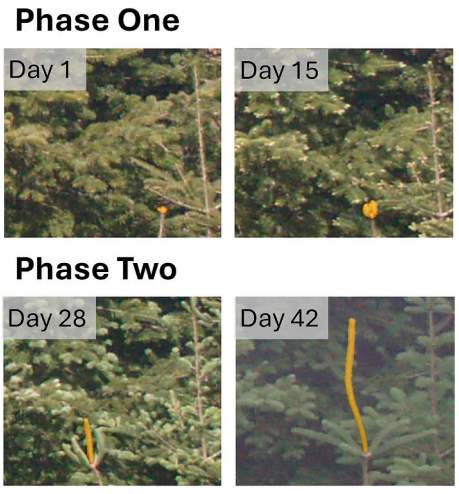

Fig. 4. Demonstration of the difference in size and shape between the early and late phase for leader LLEC 2014_24.

long as the lateral shoots. During this phase, the target bud and whorl exhibit a short and rounded shape. By the onset of phase two, the leader has elongated beyond the lateral shoots, resulting in a narrow, cylindrical shape. In our preliminary experiments in which all prompts from the entire series were applied together, the substantial change in shape between the early and late stages of leader development confused the SAM2 predictor. This initial broad approach caused the predictor to occasionally segment stem portions from the previous year's growth rather than the dormant bud in early images. This may have been because these portions were more similar in shape to the mature extended leader present in the mid- to late-season images than to the intended dormant bud.

We visually determined the timing of the end of phase one and the start of phase two for each series by noting the first date at which the lead shoot was longer than the lateral shoots. To account for the frequency of our prompts being every five days, we adjusted the timing of the start of phase two for some series to ensure that a prompt was available for the start of each phase. This was necessary to avoid propagation without an initial guiding prompt. For an example adjustment, if

the visually determined start of phase two was on the 27th image day, then since prompts were available every five image days, we designated image day 30 as the start of phase two and image day 29 as the end of phase one. Fig. 5 provides a demonstration of this. The average active time necessary for collecting prompts and visually determining the start timing of phase two was two minutes and 14 s for each leader series.

We then applied the finalized phase one prompts to the predictor and propagated the segmentation across the phase one images, and then repeated this procedure for phase two, obtaining a predicted mask for each image. Initially, we identified two issues that occasionally resulted in more than one polygon region in the raw output masks. If a nearby branch extended in front of the target leader, the predicted mask was sometimes fragmented into two pieces above and below this branch. In addition, the predicted mask occasionally included part of the stem below the target bud or shoot. To address these issues, we merged nearby fragments of the raw output masks only if they exceeded 20 px in height. Fig. 6 illustrates a sequence of processed predicted mask outputs, as well as how lateral branches from the target whorl or other trees can occlude the target mask extent.

2.3.4. Obtaining leader length time series

Finally, the leader length was estimated as the curved path length following the trajectory of the leader. As leaders often exhibited a curved posture, we used a curved path measurement rather than a simple linear height measurement. The curved path length was derived by skeletonizing the tallest connected component of each mask, thereby filtering out nearby smaller lateral shoots from the whorl. The skeleton was converted into a graph structure in which pixels were treated as nodes connected to their neighbouring pixels. Endpoints were identified either as terminal nodes of the skeleton or, when absent, as the topmost and bottommost pixels. For each skeleton component, shortest paths between all pairs of endpoints were computed, and the path with the greatest length was retained as the main leader trajectory. The curved length was then calculated as the sum of distances between successive nodes along this path. To ensure consistency with our manual reference data, we subtracted the length of the initial bud from phase one measurements as our manual reference data did not include bud length.

To guard against occasional incorrect masks, such as truncated leaders, or masks that included the stem below the target leader, we developed an outlier detection and removal protocol. We defined outliers as those having a predicted change in length of 180% of the running maximum length or more between successive days, penalizing abrupt increases, a threshold optimized through our sensitivity analysis (Table 1). We replaced outliers with interpolated values from the nearest valid lengths from within a maximum of seven days. All 105 series contained at least one outlier, and most series contained five on average.

The work of Duchesne et al. (2012) demonstrates that smoothing models such as Weibull, Gompertz, and Spline can improve the characterization of seasonal growth dynamics. Following the replacement of outliers, and prior to computing growth stage dates, we applied smoothing in the form of the Weibull function with a shape parameter equal to three to both the SAM2 and manual length series for computing phenology metrics. This smoothing method was optimized through our ablation sensitivity analysis, outperforming spline, rolling median windows, and Gompertz smoothing methods with a variety of configurations (Table 1). Note that unsmoothed data were used for computing image-level RMSE and bias metrics. Spline smoothing was performed with a smoothing factor equal to the number of values multiplied by a tuning parameter p using the UnivariateSpline() function from the SciPy interpolation package in Python 3.10.20 (Virtanen et al., 2020). Rolling median windows were applied by replacing the middle value of a window of days with the median of that window, with a step size of one day. The cumulative three-parameter Weibull function we used is as follows (Eq. 1):

$$Y(t) = A^* \left(1 - e^{-\left(\frac{t}{B}\right)^C} \right) \quad (1)$$

Where $Y(t)$ is the smoothed daily normalized length on day t, A is the asymptotic maximum normalized length (fixed at 1), B is the scale parameter corresponding to the day of year at which 63.2% of growth was attained, and C is the shape parameter controlling the curvature of the growth trajectory. The Gompertz function we used is as follows (Eq. 2):

$$Y(t) = Ae^{-B^*(t-C)} \quad (2)$$

Where $Y(t)$ is the smoothed daily normalized length on day t, A is the asymptotic maximum normalized length (fixed at 1), B is the growth-rate parameter, and C is the inflection point corresponding to the day of year at which 36.8% of growth was attained. All fitting was performed in python 3.10.20 using the curve_fit function from the SciPy optimization package (Virtanen et al., 2020).

There are several sources of uncertainty in applying SAM2 to measure leader lengths. These are conceptually presented together in an error propagation framework shown in Eq. 3.

$$\sigma^2_{\text{total}} = \sigma^2_{\text{seg}} + \sigma^2_{\text{skel}} + \sigma^2_{\text{occ}} + \sigma^2_{\text{scale}} + \sigma^2_{\text{pos}} \quad (3)$$

Where σ^2_{total} is the total uncertainty budget, σ^2_{seg} is the segmentation uncertainty component, σ^2_{skel} is the skeletonization uncertainty component, σ^2_{occ} is the occlusion uncertainty component, σ^2_{scale} is the image-scale uncertainty component, and σ^2_{pos} is the biological posture uncertainty component. These uncertainty components are difficult to quantify and isolate in practice due to confounding environmental variables. The sensitivity ablation analysis we performed alternatively enables an assessment of the influence of major adjustable workflow components on per-mask and per-series error metrics relative to leader target scene characteristics and site-level differences (Tables 1 and 2). We developed an extensive dataset for the evaluation of the influence of our SAM2 pipeline components by varying segmentation prompt frequencies, mask-cleaning procedures, outlier thresholds, and smoothing approaches across 9,792 configurations. A type II nested analysis of variance (ANOVA) for the error contributions of different pipeline components in the estimation of the timing of the 50% growth stage indicated that the pipeline was generally robust to parameter tuning, as adjustable parameters accounted for less than 3% of total variance. Instead, variance was predominantly driven by random residual noise (73%), and unique leader target scene characteristics (24%), with phase splitting being the most influential adjustable pipeline component (Table 2). A type II ANOVA for the influence of pipeline components on per-image leader length RMSE also found variance to be predominantly attributable to residual noise (57%) though with leader target scene characteristics being more important than for the per-series 50% growth error metric (38%). Phase splitting was also the most influential adjustable pipeline component for this ANOVA. The predominant

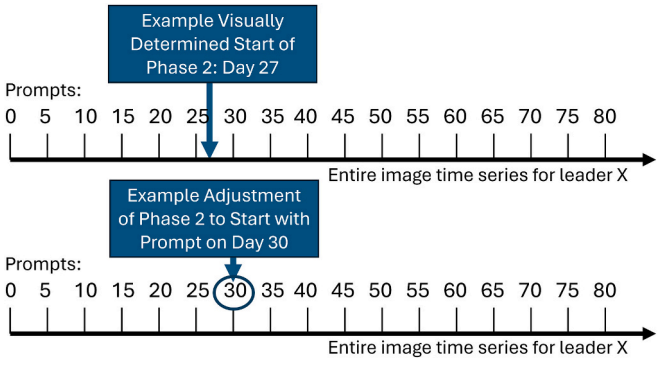

Fig. 5. Demonstration of the adjustment of phase boundaries to accommodate prompt frequency and ensure each phase began with a prompt.

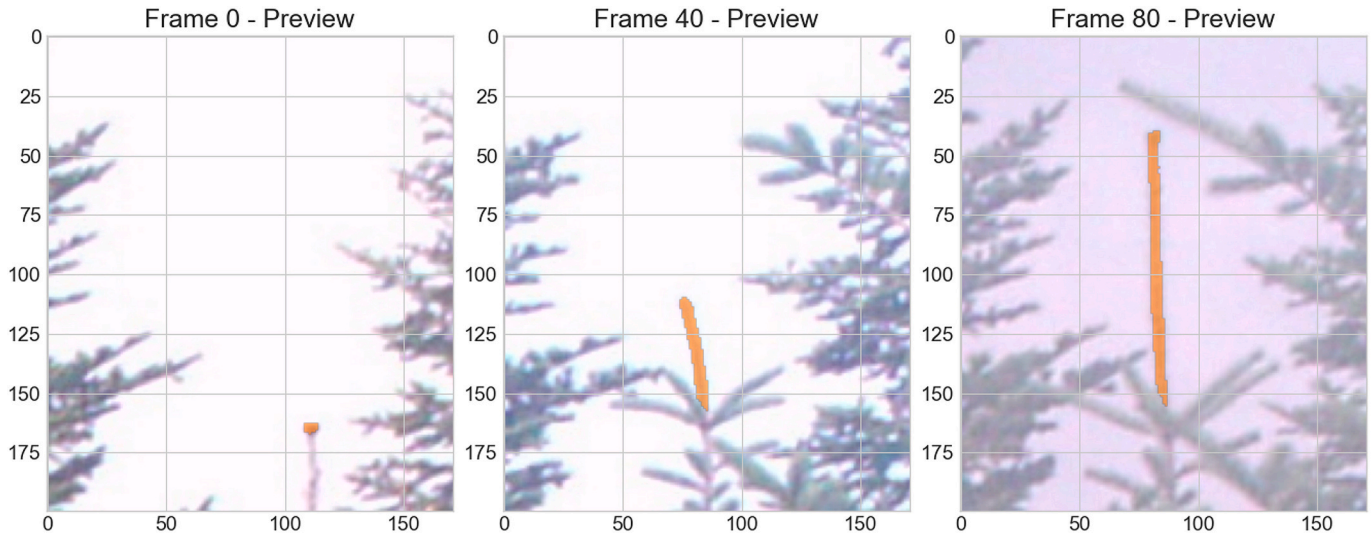

Fig. 6. Example sequence of processed predicted mask outputs for leader 21 at site LLEC in the year 2015.

Table 2
Type II analysis of variance (ANOVA) for the influence of SAM2 pipeline component configurations on per-series absolute error in the prediction of the timing of 50% growth achieved and per-image error in the form of root mean squared error (RMSE) in the estimation of leader lengths relative to the reference manual measurement approach. All values are rounded to the nearest whole number.

Environmental or SAM2 pipeline component	Explained variance in the absolute error of timing of 50% growth achieved	Explained variance in the RMSE of leader lengths
Random error	73%	57%
Leader	24%	38%
Site	1%	1%
Phase splitting	2%	4%
Smoothing	0%	–
Box spacing	0%	1%
Mask merging	0%	0%
Negative prompts	0%	0%
Outlier threshold	0%	0%

influence of residual noise across both models reflects the significant role of unresolved variables such as daily and seasonal environmental variation in lighting along with human inaccuracies in measurement and prompting. For example, Rana et al. (2026b) demonstrated that segmentation accuracy can be highly influenced by lighting variation and variable scene heterogeneity. Leader-level target scene characteristics were also significant, representing the combined influence of leader morphology, image scale, and localized background occlusions unique to each leader.

The average computational time necessary to obtain length estimates for a given leader series, including processing on average 120 images, applying on average 24 prompts to the predictor, and propagating segmentations through the time series, was 47 s. Combined with the interactive time necessary for collecting prompts and identifying the start of phase two (two minutes and 14 s), the total time necessary for extracting length estimates for each leader series was three minutes and one second on average.

2.4. Manual leader length measurements

To evaluate our SAM2 approach for leader tracking, we collected reference measurements of leader apical growth over time through manual annotation of each daily image. Two different software were used over the course of this work from 2012 to 2024. For earlier images from site LLEC, daily leader lengths for each selected tree were measured using Adobe Illustrator software (version 15.1.0). For more recent images from site LLFM, we used ImageJ software (version 1.53f). In Adobe Illustrator, daily images were stacked in layers, and the leader of each tree was traced backwards through the season using the Pen tool, starting with the final image showing the fully developed leader and ending with the first image showing only the apical bud. ImageJ was adopted for the later images because it is open-source and well suited to image sequences. We examined a subset of annual growth increments measured with both tools and found the measurements to be consistent, with minute differences due to variations in manual tracing. Only annual growth was measured, excluding the terminal bud that was already formed at the beginning of the growing season. When necessary, anchor points were added along the tracing to follow the curvature of the leader as closely as possible. The length of each traced segment (in pixels) was then measured using the "Lengths and Areas" tool of the JLG-Cotation extension (version 13.2, jlgtools.com). In ImageJ, daily images from a given year were imported as an image sequence. Similarly, leaders were traced backwards through the season using the Segmented Line tool, and the length of each segment (in pixels) was measured. Fig. 7 provides a demonstration of the leader length measurements using Adobe Illustrator and ImageJ software. The typical time required for an individual to measure the length of a leader using these techniques was approximately 30 s per image, or about one hour per leader per year with an annual series of 120 images. Note that unlike the SAM2 method, when nearby shoots or branches occluded part of the target leader as illustrated in Fig. 6, these manual approaches were robust to such obstructions, and the intended length was reliably extracted.

2.5. Comparing manual and SAM2 measurements and growth dynamics

Absolute leader lengths over time differed between trees due to inter-tree competition, variable individual performance, and position relative to the camera, among other factors. To facilitate phenology comparisons between leader time series and approaches, we normalized length values by expressing them as relative values between 0 and 100% of the maximum leader length measured for a given growing season. This normalization removed differences in absolute pixel scale between series while preserving relative growth dynamics. To quantify the agreement between manual and SAM2-derived length values for each leader time series, we computed the root mean squared error (RMSE), coefficient of determination (R^2), and bias (mean of residuals) in three evaluations: 1) estimated length for each leader image, 2) maximum length for each leader time series, and 3) the first day of the year at which 25%,

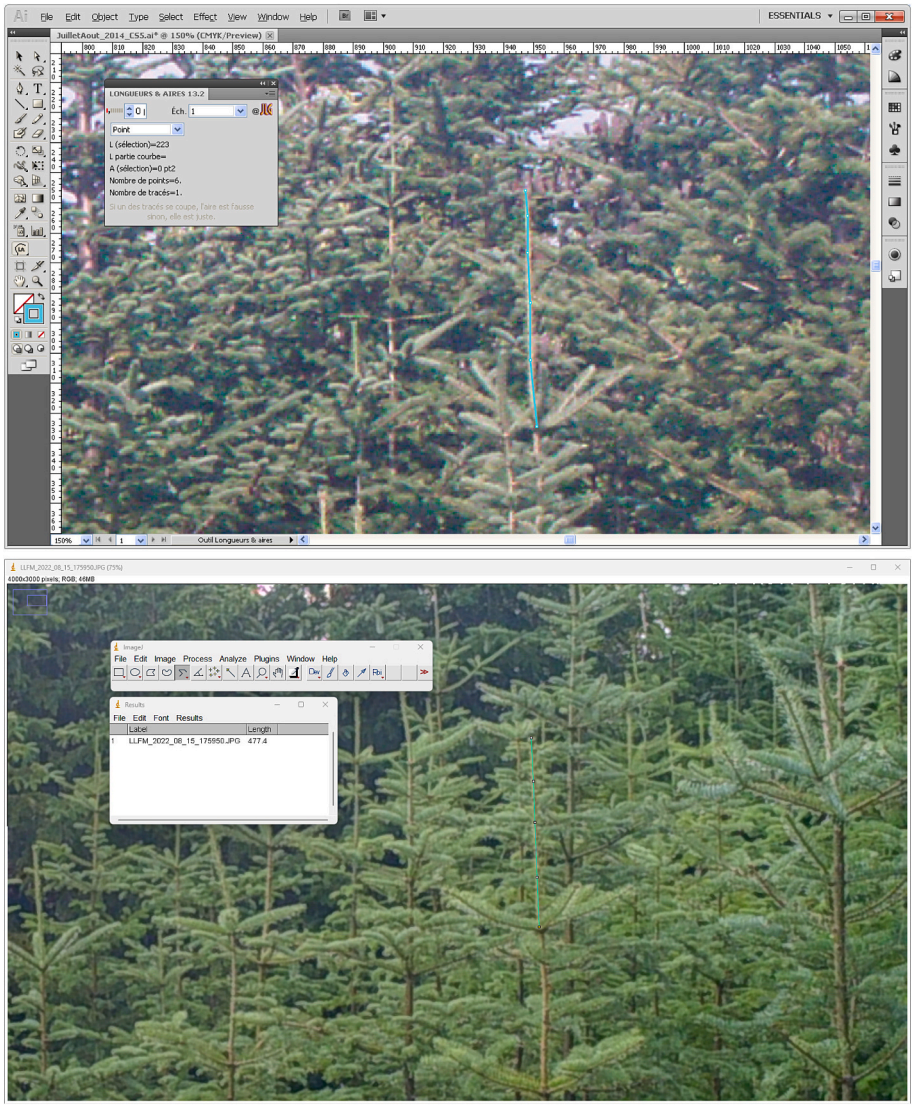

Fig. 7. Example leader length measurement using Adobe Illustrator for LLFM site in 2014 (top) and ImageJ for LLEC site in 2022 (bottom).

50%, and 75% of maximum length was reached for each leader time series. Note that the normalized values were only used for the comparison of phenology between leader time series and approaches, while all other evaluations involved absolute length values.

3. Results

Overall, the SAM2-derived leader lengths showed strong agreement with manual reference measurements (Fig. 8). Length estimates from SAM2 were reliable for both short masks (<50 px, RMSE = 5.4 px, R^2 = 0.87), corresponding to buds and whorls, and long masks (>50 px, RMSE = 19.1 px, R^2 = 0.96), corresponding to elongated leaders, despite substantial differences in shape, size, and visual features between buds and maturing leaders (overall R^2 = 0.98). Additionally, leaders with backgrounds consisting of dense balsam fir branches and shoots were tracked as reliably with SAM2 as leaders against a background of sky, despite the potential for erroneously tracking similar-looking elements. The frequency of our guiding prompts likely helped mitigate this potential limitation of SAM2.

Across leader series, there was also strong agreement between SAM2-derived and manual measurements of maximum length (R^2 = 0.98, Fig. 8). Maximum lengths varied widely among leaders and years, ranging from less than 100 px to more than 600 px. Evaluation metrics varied among camera deployments as a combined result of site differences, substantial variation in the number of images available from each camera, variable growing conditions for the years with images for each camera, as well as potential differences in camera models (Table 3). The lowest RMSE was observed for the LLEC 8 MP Stealth Cam image record, while the highest RMSE was observed for the LLFM site 12 MP Stealth Cam camera record. Given that the variables of camera type, site, year, and number of images were confounded, these differences in performance should not be interpreted as evidence of differences in camera utility.

The time series of leader lengths varied between years, though generally followed a sigmoidal pattern with an initial period of slow growth, followed by rapid growth, and then slower growth once more (Fig. 9). Growth typically began in late May or early June and was complete by mid-July. The most rapid growth typically occurred in June, with slower growth in May and July. These dynamics were well captured in SAM2-derived leader length curves, which closely followed manual measurement curves, although there was a tendency for length overestimation during the early growing period and underestimation during the late growing period.

The phenology of height growth varied substantially across leaders and years. For example, the timing of 50% growth completion ranged from mid-June to late July (Fig. 10). Compared to the other evaluations

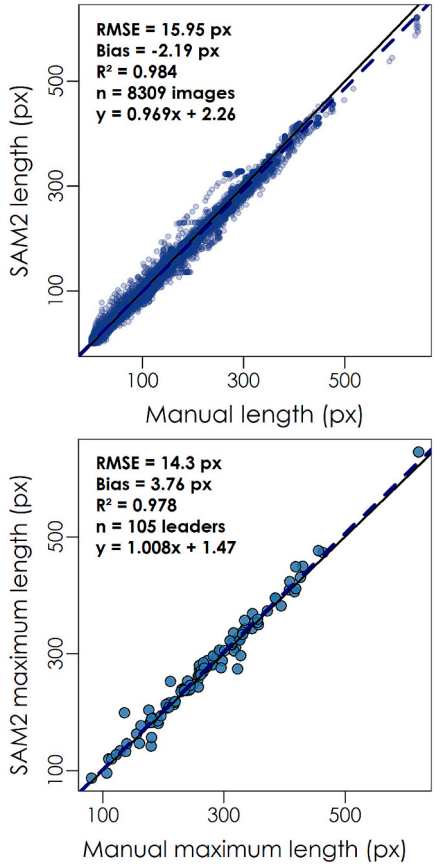

Fig. 8. Comparison of SAM2-derived leader lengths with manual measurements across all images (top) and comparison of SAM2-derived maximum leader lengths with manual measurements across all annual leader series (bottom). Points represent individual leader length measurements for each image and individual maximum leader lengths for each annual series, respectively. The dashed line represents the linear regression fit, and the solid line represents a 1:1 reference line. Displayed metrics include root mean squared error (RMSE), bias, coefficient of determination (R^2), the number of images or leaders, and the regression equation.

Table 3
Evaluation metrics for SAM2-derived lengths for different camera types used in our study.

Site and Years Used	Camera Brand and Resolution	RMSE (px)	R^2	Number of images
LLEC (2012–2020)	Stealth Cam 8 MP	11.9	0.99	5703
LLEC (2017–2018)	Stealth Cam 12 MP	12.5	0.99	334
LLFM (2018–2023)	Stealth Cam 12 MP	23.6	0.97	2112
LLFM (2024)	Spypoint 12 MP	23.0	0.99	160

based on length comparisons, the phenology of leader growth was less well captured with SAM2-derived growth curves. While bias ranged from near zero to one day across growth stages, indicating negligible systematic error, RMSE ranged from two to four days, with R^2 values from 0.79 to 0.57. Among growth stages, earlier growth stages were more reliably predicted with SAM2 than later growth stages, with the RMSE and prediction bias for the timing of 75% growth being about twice as large as those for the earlier growth stages (Fig. 10, Table 4). Bland-Altman plots revealed a uniform error distribution, with no clear trend of increasing error for earlier or later dates within growth stages (Fig. 11). The limits of agreement for the 75% growth stage were greater than those of other stages, with a span of about seven days versus four to five days, indicating greater random error for later growth stage estimates. Smoothing considerably improved phenology estimates, reducing RMSE by approximately two days for the 25% and 50% growth stages, and by approximately three days for the 75% growth stage.

To further assess whether accuracy differed for leaders with an earlier timing of 50% growth relative to later leaders, we divided leaders into two groups based on the median 50% growth date of the manual reference data, July 6 (day of year 187). Group one leaders reached 50% growth by July 6, while group two leaders reached 50% growth after July 6. The timing of 50% growth was better predicted for leaders with earlier growth ($n = 60$) than later growth ($n = 45$), with RMSE of 2.0 days versus 2.8 days, and R^2 values of 0.56 versus 0.24. We investigated each series with absolute error values of seven or more days in the estimation of growth stage timings and found that these discrepances were generally due to poor segmentations in one or more images within the series that were not caught by the outlier detection protocol. While we included an expanded range of relative outlier thresholds in our ablation sensitivity analysis, the optimal configuration did not always correctly detect such outliers across all series.

4. Discussion

4.1. Overall summary

Here we developed a novel semi-automated approach for monitoring forest growth dynamics. Using time-lapse imagery and SAM2, we can efficiently obtain accurate estimates of daily leader length. This approach performed well across a variety of contexts, including variable backgrounds, curved leaders, and different social positions of the measured tree leaders. Additionally, this technique performed well across shoot development stages, from dormant buds to fully extended mature leaders. Moreover, seasonal length series extractions using the SAM2 approach required three minutes and one second per leader series on average, including interactive and computational time. The alternative manual approaches took about one hour per leader series on average, which is about 20 times longer than the SAM2 approach.

The SAM2 pipeline developed here provides a reliable and efficient alternative to manual measurements, but it is not without limitations in terms of automation and accuracy. The workflow is not fully automated as users must provide box prompts approximately every five frames and manually identify the transition between phase one and phase two before autonomous tracking can proceed. Once these steps are completed, leader lengths can be extracted automatically. To further improve the automation of our approach, rather than manual selection of daily images, SAM2 could be applied on all hourly images or else used to automatically select one image per day with the most erect leader. While our bootstrap configuration selection and hold out validations demonstrate robustness across leaders, years, and sites sampled herein, external generalization remains to be tested. Different camera types, backgrounds, and tree social positions beyond those represented in our study may require additional validation or workflow alterations.

While there was strong overall agreement between SAM2-derived and manual length measurements ($R^2 = 0.98$), the capability of our approach for tracking phenology was more limited. There was favourable agreement for the timings of 25% and 50% growth ($R^2 = 0.79$ and $R^2 = 0.72$, respectively), though only moderate agreement for the timing of 75% seasonal growth completion ($R^2 = 0.57$). Further investigation revealed that predictions were more accurate for leaders exhibiting earlier growth than later growth. This suggests that seasonal growth dynamics are better predicted for fast-growing leaders than-slow growing leaders with SAM2.

To our knowledge, no studies have applied SAM2 or earlier versions of SAM to segment individual vegetation organs, whereas studies involving segmentation of entire plants, trees, or forest patches are more common. Rodriguez-Sanchez et al. (2025), used SAM (v1) to segment

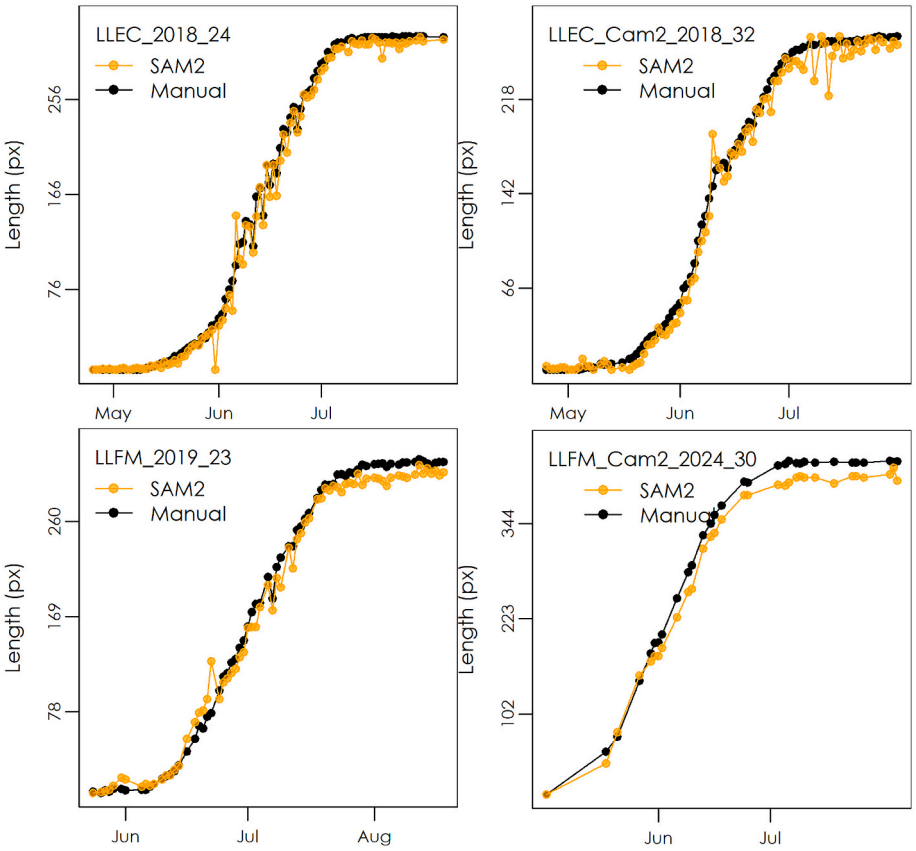

Fig. 9. Daily unsmoothed time series of SAM2 and manual-derived leader lengths for an example leader from each camera used in this study.

unmanned aerial systems (UAS) imagery of peanut plants within crop plots, leveraging SAM's fully semi-automated zero-shot segmentation capability. Despite the relatively high contrast between plants and background soil in their imagery, the authors still incorporated user refinement of the semi-automatically generated masks to ensure accurate segmentation of individual plants to address both false-positive and false-negative segmentation errors. The pipeline used in that study, while distinct from ours, suggests that even in structurally simple or high-contrast vegetation scenes, SAM-based segmentation often benefits from some degree of manual interaction, whether in the form of initial prompts or refinement of segmentation outputs. Studies such as ours, involving SAM-based segmentation over image time series, are rarer still. Tian et al. (2025) used a modified version of SAM with Sentinel-1 Synthetic Aperture Radar (SAR) data to detect forest disturbance patches in monthly aggregated imagery from 2016 to 2023. The authors incorporated point prompts to train SAM with a modified image encoder on small, labelled SAR patches, including local fine-tuning for different regions and detection of disturbance from monthly output based on a threshold applied to five-month aggregated time series. Although their work differs from ours in spatial scope, image type, and temporal resolution, the pipelines are conceptually similar: both require user guidance at key stages, ours being in the form of prompts and phase delineations, and theirs through regional fine-tuning, and both apply filtering to stabilize model predictions over time.

4.2. Applications: Genotype selection, tracking needleleaf phenology, and large-scale monitoring

To the best of our knowledge, this is the first implementation of semi-automated, high-frequency, vertical tree growth monitoring. This high-frequency monitoring approach can support a wide range of forestry and research applications. For example, trials aimed at quantifying height growth rates and climate responses among different tree species, provenances, and genotypes currently necessitate manual measurement campaigns. Height growth can occur rapidly and sporadically, with growth rates varying considerably from day to day throughout the growing season. Manual field measurement campaigns therefore present several limitations, including their infrequency relative to the daily nature of potential growth increments, their labour-intensive and costly nature, and their susceptibility to human measurement error. Our SAM2-based technique could alleviate these limitations by providing frequent, cost-effective, and precise estimates of seedling and sapling height over time.

In addition, the reliability of our workflow for extracting relative pixel-based measurements suggests that this workflow could be extended to obtain absolute measurements. While not tested in the current study, relative pixel-based measurements may be translated into absolute measurements using a single field calibration of a mature shoot, or by installing a reference object of known length within the same region of the image as the target leader. To calibrate pixel measurements for each leader, we recommend performing a single field measurement of each leader of interest within the image field of view at mature length. This local calibration may help to account for variable effects of lens distortion and camera distance across the image field of view by conducting calibration measurements for each leader of interest in the region of the image in which it presides. Alternatively, to minimize field visits, a reference object of known size can be installed next to the target leader during camera installation so that it appears in all cropped images. The size of this object may then be used to convert pixel measurements of the nearby leader into absolute length measurements. Due to the potential for oblique curvature relative to the camera perspective, this approach requires careful selection of images to obtain reliable absolute length estimates. It is important to note that camera distance, lens distortion, and differing leader orientations relative to the image

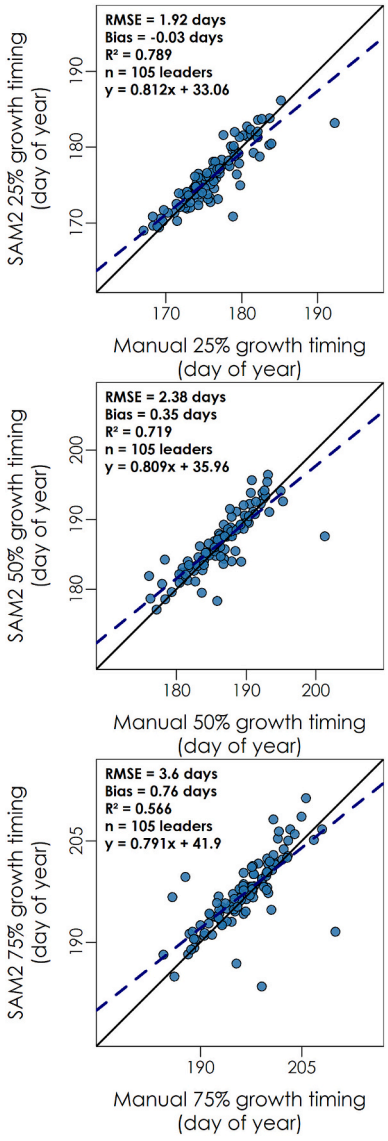

Fig. 10. Comparison of the timing of 25%, 50%, and 75% of annual growth between SAM2-derived leader lengths and manual measurements across leader image time series. Points represent individual percentage growth day-of-year values, the dashed line represents the linear regression fit, and the solid line represents the 1:1 reference line. Displayed metrics include root mean squared error (RMSE), bias, coefficient of determination (R^2), the number of leader time series, and the regression equation.

Table 4
Bias between manual and SAM2-derived growth stage dates.

Growth Stage	Timing Bias ± 95% Confidence Interval (days)
25%	−0.03 ± 0.28
50%	0.35 ± 0.37
75%	0.76 ± 0.57

plane, along with occlusion can together bias segmentation derived measurements such as apparent length (Rana et al., 2026a). Note that in cases of branches occluding the target leader, we recommend the use of manual measurements or else a carefully selected outlier threshold and removal protocol. Adapting our approach for tracking the vertical growth of seedlings is currently under development for the TransX project which involves the planting and monitoring of more than 85,000 seedlings (Ravn et al., 2026). This application presents additional challenges and opportunities, with lower resolution images and a larger target in the form of a seedling rather than an apical bud or leader. Looking forward, SAM developments are ongoing, and SAM version 3 (SAM3) will allow users to incorporate text prompts alongside other guiding prompts, providing further opportunities to improve both accuracy and automation (Carion et al., 2025).

Stationary time-lapse cameras installed at the tree- or canopy-level, also known as phenocams, are commonly used to monitor the timing of leaf emergence and senescence for deciduous trees but cannot be used to identify the same discrete events for evergreen trees. The rising greenness signal extracted from phenocam observations of evergreen conifers results from both the greening of existing needles and the emergence of new needles. This limits the utility of phenocams for precisely detecting the timing of evergreen needle emergence (Seyednasrollah et al., 2021). Until now, to confidently distinguish between the timing of greening of existing needles and the emergence of new needles, additional field measurements and observations were necessary alongside phenocam analysis protocols (Zhang et al., 2020). Our SAM2-monitoring approach could provide a semi-automated alternative for tracking the emergence of new needles from dormant buds and distinguishing it from the greening of existing needles. This primary growth monitoring could be performed without the deployment of additional equipment beyond the time-lapse-capable cameras already used for phenocam applications.

To determine whether the precision of our phenology estimates is sufficient, we considered two phenology tracking applications: 1) secondary growth phenology and 2) leaf phenology. Studies of secondary growth phenology including xylogenesis often involve weekly dendroband or sub-daily point dendrometer measurements which are filtered to isolate irreversible growth from reversible daily shrinkage and swelling. Estimated growth stage dates are then often compared to dates derived from cellular analyses of microcore samples collected on a weekly basis, with a target precision of roughly ±7 days (Dow et al., 2022; Jankowski et al., 2025; Zeng et al., 2022). Leaf phenology may be tracked with sub-daily phenocam images or less frequent satellite-based observations. Within phenocam pipelines estimated leaf phenophases are often extracted from thresholds applied to filtered vegetation indices and compared to weekly or sub-weekly ground observations, with uncertainty intervals ranging from about five days to more than a week (Delpierre et al., 2020; Keenan et al., 2014; Richardson et al., 2018; Zhang et al., 2018). The Bland-Altman limits of agreement for the SAM2 method were ± 4 and ± 5 days for the 25% and 50% growth stages, though up to ±7 days for the 75% growth stage (Fig. 11). These limits are consistent with the seven-day precision threshold for secondary growth phenology studies, though the higher error random error for the 75% growth stage may exceed the target precision threshold for phenocam studies. To improve the reliability of SAM2 methods for distinguishing genotype growth stage timings, we recommend that comparison studies include multiple replicates per genotype to account for random error. In addition, the work of Rana et al. (2026a) warrants further investigation into the influence of spectral variability and lighting heterogeneity on image-based phenology predictions.

Airborne and terrestrial laser scanning techniques for monitoring forest height and radial tree growth often necessitate frequent and extensive manual field measurement campaigns using tools such as clinometers and calipers for validation and reference measurements (Soininen et al., 2024; Yrttimaa et al., 2023). Our SAM2-based monitoring approach, combined with dendrometer measurements, could complement these remote sensing methods. Installing co-located cameras and dendrometers across monitored forests could reduce the labour involved in obtaining reference measurements and minimize human error. In addition, the near-continuous radial and height growth time series these sensors could generate would allow for the investigation of intraseasonal growth dynamics in the context of environmental changes.

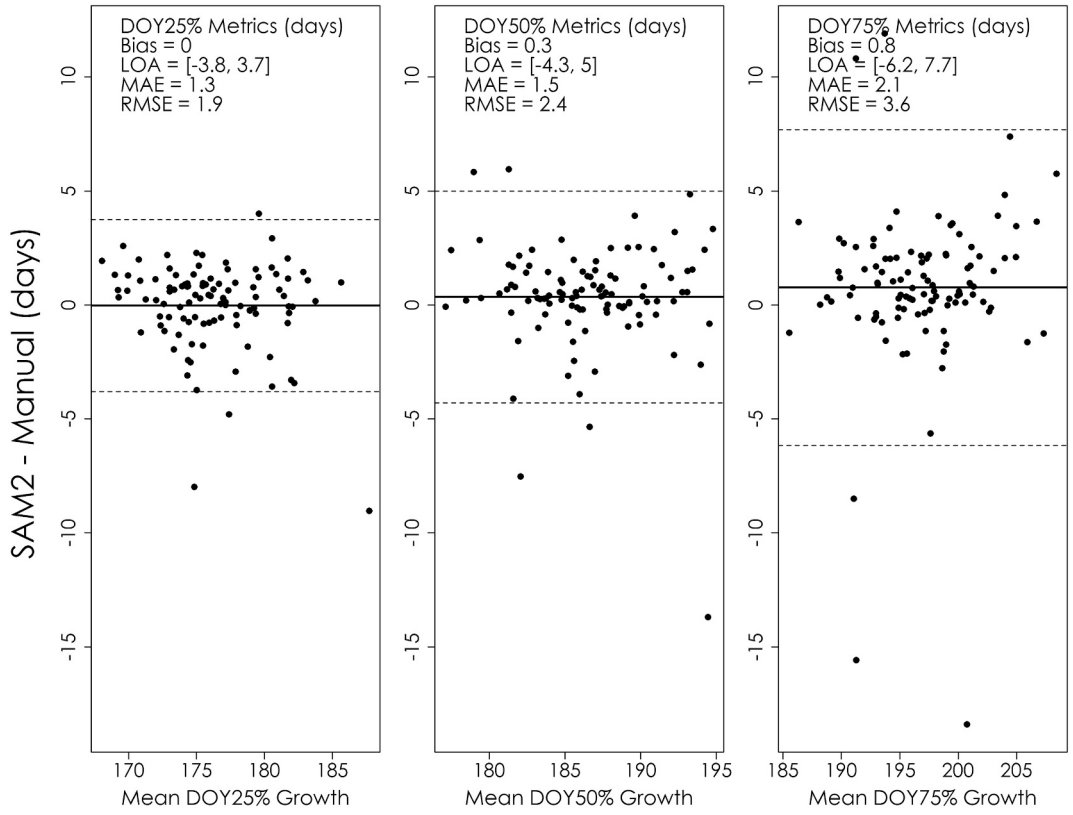

Fig. 11. Bland-Altman analysis of the limits of agreement (LOA) in units of days between SAM2-derived and manually derived estimates of the timing of 25%, 50%, and 75% seasonal growth. Solid lines indicate mean bias and dashed lines indicate the 95% limits of agreement.

4.3. Challenges & avenues for improvement

During dry periods in seasonal and daily cycles, reduced turgor pressure in balsam fir shoots can lead to increased shoot curvature. If shoots curve at an oblique angle, either toward or away from the camera, this can hinder the accurate measurement of true shoot length using our approach. This artefact could lead to an underestimation on a given day followed by overestimation of growth on subsequent days when turgor pressure increases and the stem straightens. This issue can be mitigated by selecting images acquired in the early morning or late in the day rather than at mid-day or in the afternoon, as shoots typically exhibit greater turgor pressure during these periods. In addition, it is beneficial to limit camera movement throughout the season for the collection of manual reference measurements from image time series, though SAM2 is robust to camera movement, provided the target leader is still in the camera field of view. While the curvature of shoots presents a limitation in our current framework, it could also offer an opportunity for another avenue of tree physiology monitoring. Anomalous predicted declines in length or vertical extent could be indicative of instances of reduced turgor pressure.

With reliable time series of emergent shoot lengths, the timing and environmental context of productive growth days can be investigated, enabling a better understanding of the phenology and drivers of intra-seasonal primary growth. However, our SAM2-based monitoring approach only achieved moderate agreement with reference measurements for the timing of 75% of seasonal growth. To obtain more reliable estimates of the timing of different growth stages, users could review and refine SAM2 mask predictions by applying additional positive and negative prompts throughout the image time series as needed. This could also potentially help to address cases of obstruction as demonstrated in Fig. 6, though in some cases feature selection may be challenged by lateral obstruction with adjacent branches or shoots. To address these cases, a hybrid approach involving occasional manual measurements or mask delineations may be needed in combination with SAM2.

4.4. Future work

Balsam fir is a fitting candidate for primary growth monitoring using time-lapse photography and SAM2 due to its strong apical dominance. For robust assessments of stand-level growth patterns, our approach could be adapted for tracking primary growth in other species, including broadleaf deciduous and other evergreen needleleaf species. As our approach performed well across a variety of target shapes, from small rounded dormant buds to long cylindrical leaders, its applicability to species with diverse morphologies, leaf types, and branching structures is promising. In addition, our approach could be extended to track seedling growth from image time series, such as those generated by the TransX project and other emerging monitoring networks. Such developments would provide timely insights to support the selection of climate-resilient forest species for nature-based climate solutions and forest management.

5. Conclusion

Here we developed and evaluated a novel semi-automated approach for monitoring fine-scale height growth of young balsam fir trees using daily time-lapse imagery and the Segment Anything Model v2 (SAM2; Meta AI Research). Guiding prompts were provided every five images to track the development of a dormant apical bud into a mature extended leader throughout each of 105 annual image series. We observed strong agreement between SAM2-derived shoot lengths and reference measurements obtained via manual annotation of each image ($R^2 = 0.98$, $n = 8{,}309$ images). On average, the SAM2 approach was 20 times faster than the manual reference method for each leader series. Agreement between SAM2-derived and manual estimates of the timing of 75%

growth amplitude was more moderate ($R^2 = 0.57$). Future applications could improve phenological accuracy by incorporating intermittent refinement of SAM2 predicted masks where necessary. To our knowledge, this represents the first semi-automated in-situ approach for tracking fine-scale height growth. This monitoring framework provides timely opportunities for forestry researchers and practitioners to establish species- and provenance-specific height growth phenology profiles, supporting climate-resilient forest management.

CRediT authorship contribution statement

Lynsay Spafford: Visualization, Software, Methodology, Formal analysis, Data curation, Conceptualization. **Louis Duchesne:** Writing – review & editing, Resources, Investigation, Funding acquisition, Formal analysis, Data curation. **Vivien Sainte Fare Garnot:** Writing – review & editing, Formal analysis. **Jacob Ravn:** Writing – review & editing. **Loïc D'Orangeville:** Writing – review & editing, Funding acquisition, Formal analysis.

Ethics approval

All authors certify that no humans or animals were involved in this study.

Declaration of competing interest

The authors declare no conflicts of interest.

Acknowledgements

We acknowledge the support of Research Nova Scotia through a 2023-2024 Forestry Award (#2023-2485) as well as the Natural Sciences and Engineering Research Council of Canada (NSERC; funding reference number PDF – 585344–2024). Field work was funded by the Ministère des Ressources naturelles et des Forêts du Québec through project number 112332064.

Data availability

Data and code available at doi: https://doi.org/10.5061/dryad.j9kd51ct9.

References

Aldea, J., Bravo, F., Vázquez-Piqué, J., Rubio-Cuadrado, A., del Río, M., 2018. Species-specific weather response in the daily stem variation cycles of Mediterranean pine-oak mixed stands. Agric. For. Meteorol. 256, 220–230.

Aldea, J., Bravo, F., Vazquez-Pique, J., Ruiz-Peinado, R., del Rio, M., 2021. Differences in stem radial variation between Pinus pinaster ait and Quercus pyrenaica Willd may release inter-specific competition. For. Ecol. Manag. 481, 118779.

Carion, N., Gustafson, L., Hu, Y.-T., Debnath, S., Hu, R., Suris, D., Ryali, C., Alwala, K.V., Khedr, H., Huang, A., 2025. Sam 3: Segment Anything with Concepts arXiv preprint arXiv:2511.16719.

Claveau, Y., Messier, C., Comeau, P.G., Coates, K.D., 2002. Growth and Crown Morphological Responses of Boreal Conifer Seedlings and Saplings with Contrasting Shade Tolerance to a Gradient of Light and Height. cdnsciencepub.com, 32, pp. 458–468. https://doi.org/10.1139/X01-220.

Delpierre, N., Soudani, K., Berveiller, D., Dufrêne, E., Hmimina, G., Vincent, G., 2020. "Green pointillism": detecting the within-population variability of budburst in temperate deciduous trees with phenological cameras. Int. J. Biometeorol. 64, 663–670.

D'Orangeville, L., Itter, M., Kneeshaw, D., Munger, J.W., Richardson, A.D., Dyer, J.M., Orwig, D.A., Pan, Y., Pederson, N., 2022. Peak radial growth of diffuse-porous species occurs during periods of lower water availability than for ring-porous and coniferous trees. Tree Physiol. 42, 304–316.

Dow, C., Kim, A.Y., D'Orangeville, L., Gonzalez-Akre, E.B., Helcoski, R., Herrmann, V., Harley, G.L., Maxwell, J.T., McGregor, I.R., McShea, W.J., 2022. Warm springs alter timing but not total growth of temperate deciduous trees. Nature 608, 552–557.

Duchesne, L., Houle, D., D'Orangeville, L., 2012. Influence of climate on seasonal patterns of stem increment of balsam fir in a boreal forest of Québec, Canada. Agric. For. Meteorol. 162, 108–114.

Etzold, S., Sterck, F., Bose, A.K., Braun, S., Buchmann, N., Eugster, W., Gessler, A., Kahmen, A., Peters, R.L., Vitasse, Y., 2022. Number of growth days and not length of the growth period determines radial stem growth of temperate trees. Ecol. Lett. 25, 427–439.

Hattula, E., Raninen, J., Zhu, L., 2025. Segment anything model with LiDAR based images for building segmentation in forest areas. Int. Arch. Photogramm. Remote. Sens. Spat. Inf. Sci. 48, 13–19.

Hu, X., Xu, X., Shi, Y., 2023. How to Efficiently Adapt Large Segmentation Model (SAM) to Medical Images arXiv preprint arXiv:2306.13731.

Jankowski, P.A., Calama, R., Aldea, J., García, M., Madrigal, G., Pardos, M., 2025. Improving phenological event identification in trees using manually measured dendrometer data: conventional approaches vs. the novel two-stage threshold approach. Front. For. Glob. Change 8, 1589579.

Kattenborn, T., Fassnacht, F.E., Pierce, S., Lopatin, J., Grime, J.P., Schmidtlein, S., 2017. Linking plant strategies and plant traits derived by radiative transfer modelling. J. Veg. Sci. 28, 717–727. https://doi.org/10.1111/jvs.12525.

Keenan, T.F., Darby, B., Felts, E., Sonnentag, O., Friedl, M.A., Hufkens, K., O'keefe, J., Klosterman, S., Munger, J.W., Toomey, M., 2014. Tracking forest phenology and seasonal physiology using digital repeat photography: a critical assessment. Ecol. Appl. 24, 1478–1489.

Kershaw, J.A., Ducey, M.J., Beers, T.W., Husch, B., 2016. Forest mensuration. John Wiley & Sons.

Kneeshaw, D.D., Kobe, R.K., Coates, K.D., Messier, C., 2006. Sapling size influences shade tolerance ranking among southern boreal tree species. J. Ecol. 471–480.

Niinemets, Ü., Valladares, F., 2006. Tolerance to shade, drought, and waterlogging of temperate northern hemisphere trees and shrubs. Ecol. Monogr. 76, 521–547.

Olsson, M., 2024. Early Detection of Bark Beetle Attacks: Integrating Segment Anything Model (SAM) Zero-Shot Segmentation and Spectral Indices for Tree Health Assessment. Student thesis series INES.

Oogathoo, S., Duchesne, L., Houle, D., Kneeshaw, D., Bélanger, N., 2024. Precipitation and relative humidity favours tree growth while air temperature and relative humidity respectively drive winter stem shrinkage and expansion. Front. For. Glob. Change. 7, 1368590.

Pappas, C., Peters, R.L., Fonti, P., 2020. Linking variability of tree water use and growth with species resilience to environmental changes. Ecography 43, 1386–1399.

Que, H., Gao, H., Shan, W., Liu, M., An, J., Deng, F., Feng, S., Yang, X., Mu, L., 2026. FM-SAM: individual tree crown delineation and classification based on Segmentation Anything Model (SAM) and YOLOv10 in UAV imagery for forest monitoring. Comput. Electron. Agric. 240, 111162.

Rana, S., Hensel, O., Nasirahmadi, A., 2026a. From vineyard to vision: multi-domain analysis and mitigation of grape cluster detection failures in complex viticultural environments. Results Eng. 29, 108833. https://www.sciencedirect.com/science/article/pii/S2590123025048765.

Rana, S., Hensel, O., Nasirahmadi, A., 2026b. Generative semantic reconstruction for annotation-ready vegetation priors in spectrally heterogeneous rangeland imagery. MethodsX 16, 103967. https://www.sciencedirect.com/science/article/pii/S2215016126001858.

Ravi, N., Gabeur, V., Hu, Y.-T., Hu, R., Ryali, C., Ma, T., Khedr, H., Rädle, R., Rolland, C., Gustafson, L., 2024. Sam 2: Segment anything in Images and Videos arXiv preprint arXiv:2408.00714.

Ravn, J., Moreau, G., Mayrinck, R., Itter, M., Albert, C., Spafford, L., Kneeshaw, D., Achim, A., Perron, M., Dumont, S., Rogers, G., D'Orangeville, L., 2026. The TransX project: a latitudinal network of provenance trials across eastern North America to test the climatic vulnerability of northeastern tree species and their potential for assisted migration. Forest. Chron. 102, 6–14.

Richardson, A.D., Hufkens, K., Milliman, T., Aubrecht, D.M., Chen, M., Gray, J.M., Johnston, M.R., Keenan, T.F., Klosterman, S.T., Kosmala, M., 2018. Tracking vegetation phenology across diverse North American biomes using PhenoCam imagery. Sci. Data 5, 1–24.

Rodriguez-Sanchez, J., Da Silva, R.M., Chu, Y., Rodriguez, L., Zhang, J., Johnsen, K., Ozias-Akins, P., Li, C., 2025. Aerial imagery and segment anything model for architectural trait phenotyping to support genetic analysis in peanut breeding. Plant Phenom. 7, 100126. https://www.sciencedirect.com/science/article/pii/S2643651525001323.

Seyednasrollah, B., Bowling, D.R., Cheng, R., Logan, B.A., Magney, T.S., Frankenberg, C., Yang, J.C., Young, A.M., Hufkens, K., Arain, M.A., 2021. Seasonal variation in the canopy color of temperate evergreen conifer forests. New Phytol. 229, 2586–2600.

Soininen, V., Hyyppä, E., Muhojoki, J., Luoma, V., Kaartinen, H., Lehtomäki, M., Kukko, A., Hyyppä, J., 2024. Accuracy comparison of terrestrial and airborne laser scanning and manual measurements for stem curve-based growth measurements of individual trees. Sci. Remote Sens. 9, 100125.

Thivierge-Lampron, J., Girona, M.M., Pappas, C., Duchesne, L., Chavardès, R.D., Balducci, L., Lemay, M.-A., Peters, R.L., Gennaretti, F., 2025. Stem water storage dynamics of three boreal tree species under short-term drought. Forests 16, 1448.

Thomas, B.R., Stoehr, M., Schreiber, S.G., Benowicz, A., Schroeder, W.R., Soolanayakanahally, R., Stefner, C., Elliott, K.A., Philis, N., Roubal, N., 2024. Tree improvement in Canada–past, present and future, 2023 and beyond. For. Chron. 100, 59–87.

Tian, Y., Zhao, F., Meng, R., Sun, R., Zhang, Y., Shen, Y., Wang, B., Liu, J., Li, M., 2025. A vision foundation model-based method for large-scale forest disturbance mapping using time series Sentinel-1 SAR data. Remote Sens. Environ. 325, 114775.

van der Maaten, E., Pape, J., van der Maaten-Theunissen, M., Scharnweber, T., Smiljanić, M., Cruz-García, R., Wilmking, M., 2018. Distinct growth phenology but similar daily stem dynamics in three co-occurring broadleaved tree species. Tree Physiol. 38, 1820–1828.

Vepakomma, U., St-Onge, B., Kneeshaw, D., 2011. Response of a boreal forest to canopy opening: assessing vertical and lateral tree growth with multi-temporal lidar data. Ecol. Appl. 21, 99–121.
Virtanen, P., Gommers, R., Oliphant, T.E., Haberland, M., Reddy, T., Cournapeau, D., Burovski, E., Peterson, P., Weckesser, W., Bright, J., 2020. SciPy 1.0: fundamental algorithms for scientific computing in Python. Nat. Methods 17, 261–272.
Wołk, K., Niklewski, J., Kopczyński, M., Tatara, M.S., Żero, O., 2025. Enhancing semantic forestry segmentation through advanced preprocessing with ML models. IEEE Access 13, 98602–98621.
Yrttimaa, T., Luoma, V., Saarinen, N., Kankare, V., Junttila, S., Holopainen, M., Hyyppä, J., Vastaranta, M., 2022. Exploring tree growth allometry using two-date terrestrial laser scanning. For. Ecol. Manag. 518, 120303.
Yrttimaa, T., Junttila, S., Luoma, V., Calders, K., Kankare, V., Saarinen, N., Kukko, A., Holopainen, M., Hyyppä, J., Vastaranta, M., 2023. Capturing seasonal radial growth of boreal trees with terrestrial laser scanning. For. Ecol. Manag. 529, 120733.
Zeng, Q., Khan, A., Deslauriers, A., Rossi, S., 2022. May temperature drives cambial resumption in the boreal black spruce. Forests 13, 2168.
Zhang, X., Jayavelu, S., Liu, L., Friedl, M.A., Henebry, G.M., Liu, Y., Schaaf, C.B., Richardson, A.D., Gray, J., 2018. Evaluation of land surface phenology from VIIRS data using time series of PhenoCam imagery. Agric. For. Meteorol. 256, 137–149.
Zhang, S., Buttò, V., Khare, S., Deslauriers, A., Morin, H., Huang, J.-G., Ren, H., Rossi, S., 2020. Calibrating PhenoCam data with phenological observations of a black spruce stand. Can. J. Remote. Sens. 46, 154–165.
Zweifel, R., Haeni, M., Buchmann, N., Eugster, W., 2016. Are trees able to grow in periods of stem shrinkage? New Phytol. 211, 839–849.
Zweifel, R., Etzold, S., Basler, D., Bischoff, R., Braun, S., Buchmann, N., Conedera, M., Fonti, P., Gessler, A., Haeni, M., 2021a. TreeNet–the biological drought and growth indicator network. Front. For. Glob. Change. 4, 776905.
Zweifel, R., Sterck, F., Braun, S., Buchmann, N., Eugster, W., Gessler, A., Häni, M., Peters, R.L., Walthert, L., Wilhelm, M., 2021b. Why trees grow at night. New Phytol. 231, 2174–2185.